

IN-SITU CHARACTERISATION OF SMALL BLUE ROUND CELL TUMOR PROTEOME AND N-GLYCOME

Christine Bollwein¹, Kristina Schwamborn¹, Thao Tran², Alice Ly², N. Heath Patterson³, Juliana P. Gonçalves¹

¹Institute of Pathology, School of Medicine, Technical University of Munich, Munich, Germany
²Aspect Analytics NV, Gent, Limburg, Belgium

Introduction

Small blue round cell tumors (SBRCT) is an umbrella term for different tumor types with similar histological presentation that can originate from entirely different tissues. Correct diagnosis is crucial as treatment strategies and prognosis vary significantly between tumor entities. However, morphological characterization of SBRCT is challenging, and routine immunohistochemistry alone is often insufficient to define them. Glycan expression profiles are potentially useful in stratifying different tumors as glycosyltransferase enzymatic activity and gene expression are altered in tumor development, where aberrant glycosylation is primarily characterized by an elevated

branching of *N*-glycans^[1]. Matrix-assisted laser desorption/ionization (MALDI) mass spectrometry imaging (MSI) is a label-free analytical technique to analyze and visualize the spatial distribution of different classes of molecules, such as peptides, glycans, lipids, and metabolites. In this study, MALDI-MSI was used to profile tryptic peptides and *N*-glycans from archival SBRCTs samples. The data was used to create classification algorithms to reliably distinguish the different entities and to identify discriminatory features between the tumor types.

Methods:

SBRCT cases (n = 26) were assembled in a tissue microarray: Ewing sarcoma (EWS, n = 5), rhabdomyosarcoma (RMS, n = 5), neuroendocrine carcinoma (NEC, n = 5), acute lymphoblastic leukemia/lymphoma (ALL, n = 5), nephroblastoma (NEPB, n = 3), and neuroblastoma (NEUB, n = 3). Every case was represented by 3 to 4 tissue cores to account for tumor variability. One TMA section was subjected to on-tissue N-glycosidase F enzymatic digestion, and a second section with trypsin, followed by matrix application and measurement on a mass spectrometer (rapifleX, Bruker)^[2]. Afterwards, the sections were H&E stained, digitized and underwent histopathological annotation (QuPath, version 0.4.3).

Data analysis was performed using SCILS Lab (Bruker, v.2024a), Weave (v.1.0, Aspect Analytics), and Python (v.3.9). Weave was used to co-register all datasets, combining the peptide and glycan data into a single dataset for comparison of analytes and histology, and interactive assessment of data analysis. A schematic of the entire workflow is shown in figure 1.

Classification of data according to the different tumor types was performed on pixel (i.e. spectral) level and as a 10-fold cross-validation, using four different machine learning algorithms: gradient boosting (GB), support vector machine (SVM), k-nearest neighbor (KNN), and linear discriminant analysis (LDA). For each of the ten folds or splits, 90% of the data was used for algorithm training, with the remaining 10% reserved as a test set. Every iteration yielded statistical scores, the average of them resulted in the final scores.

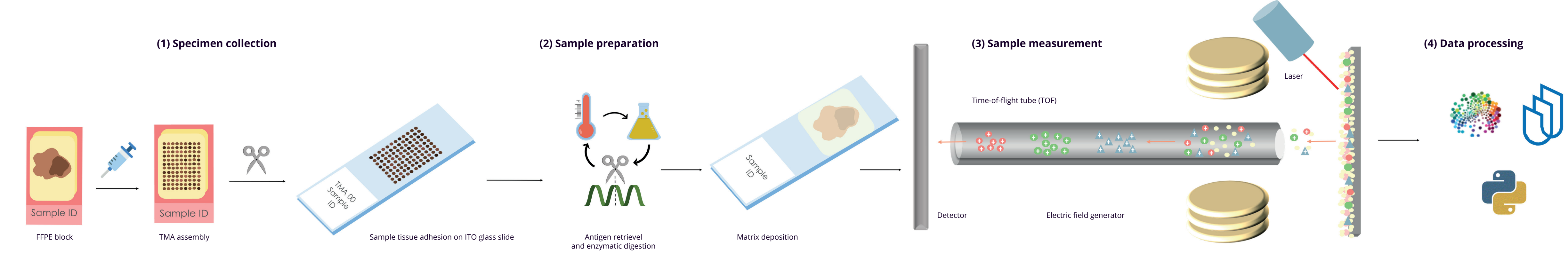


Figure 1: Schematic showing workflow from sample processing to mass spectrometry imaging data acquisition and data analysis

Results

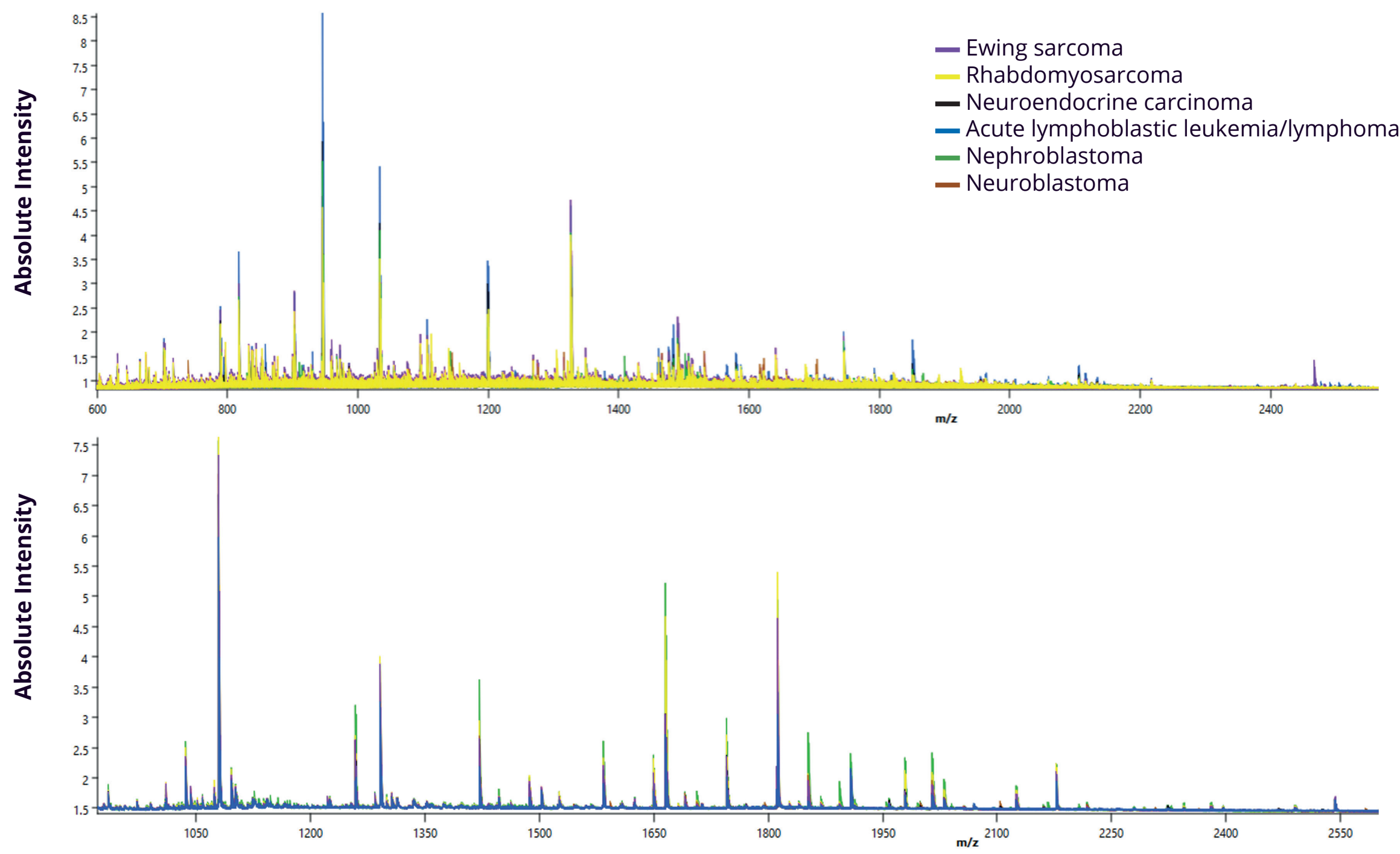


Figure 2: Different SBRCT types produce different mass spectra. Summary showing average spectra for (A) tryptic peptides and (B) *N*-glycans for each of the six SBRCT types. Inset: colour key for the different SBRCT subtypes.

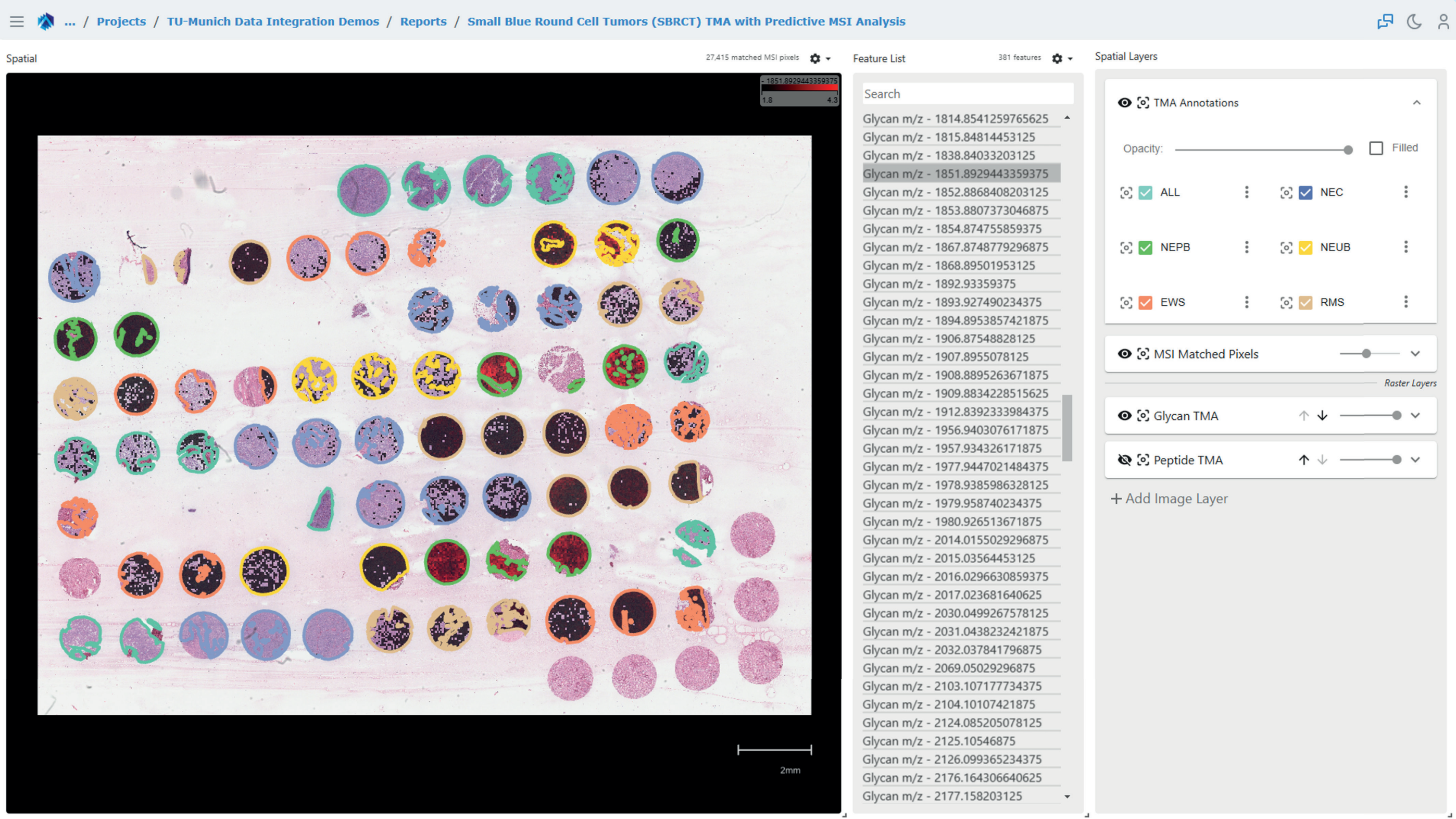


Figure 3: Weave report showing joint visualization of the MALDI-MSI datasets, H&E microscopy and pathology annotations. This allows visualisation of *m/z* localisations and intensities in the tissue relative to SBRCT subtype and tumor regions. *N*-glycan *m/z* 1851.893 (red) is highest in tumor regions of subtype nephroblastoma (NEPB, annotated in light green), and lowest in acute lymphoblastic leukemia/lymphoma (ALL, annotated in cyan).

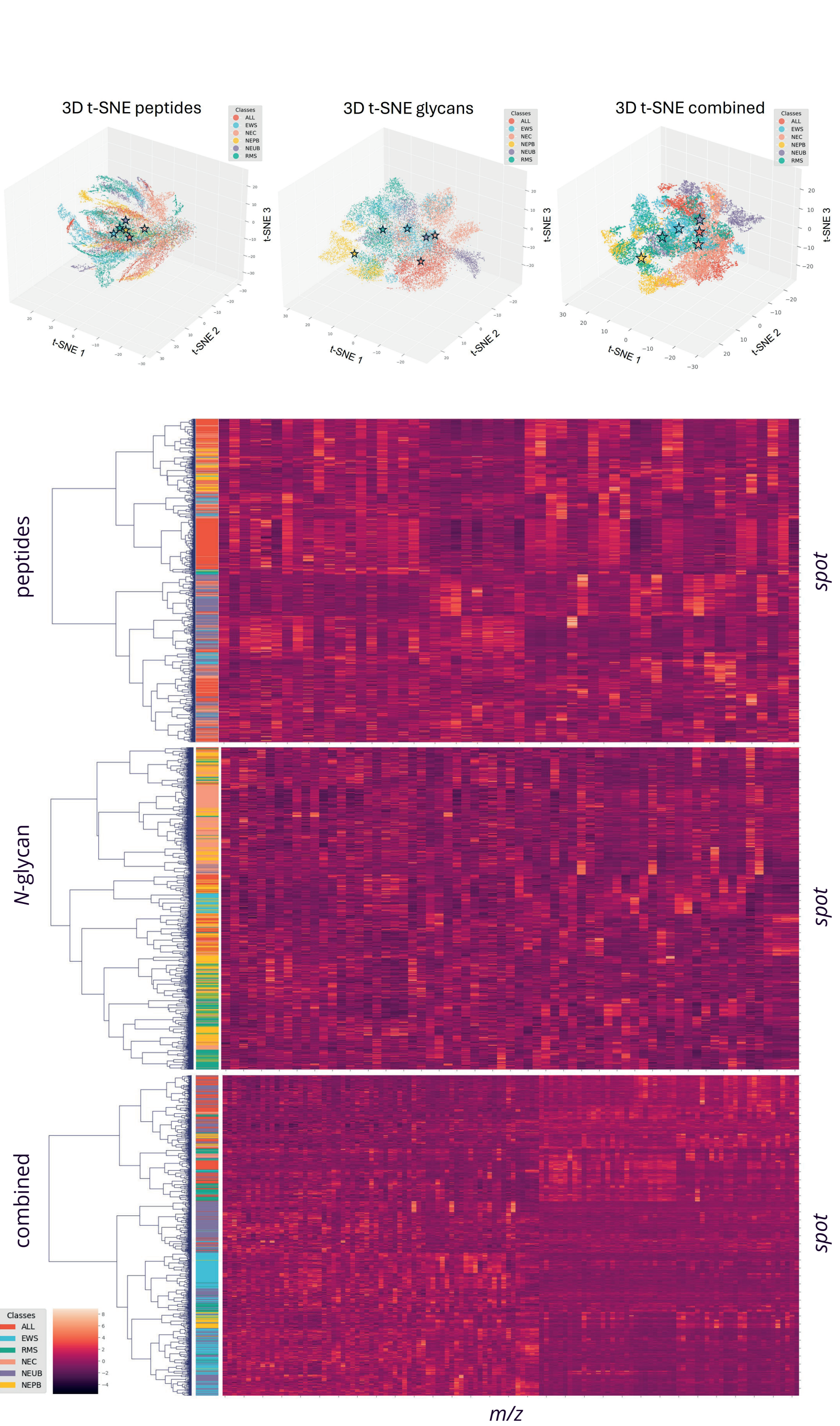


Figure 4: Top: t-SNE plots of peptide (left), *N*-glycan (center), and combined dataset (right) with different color coding of the individual classes. Clear differentiation of the respective tumor classes is evident, whereby the density and demarcation of the clusters is lowest for the peptides, increases significantly for the *N*-glycans, and is best for the combined dataset. Bottom: Hierarchical cluster analysis on the z-score normalized data of the peptide (top), *N*-glycan (center), and combined data (bottom). This also reveals a separation of the spectra regarding the tumor classes.

Table 1: Results of the one vs. rest classification strategy for each individual classifier. GB: gradient boosting, SVM: support vector machine, KNN: k-nearest neighbor, LDA: linear discriminant analysis.

	One vs. Rest											
	peptide				<i>N</i> -glycan				peptide and <i>N</i> -glycan combined			
	GB	SVM	KNN	LDA	GB	SVM	KNN	LDA	GB	SVM	KNN	LDA
EWS vs. rest	0.86	0.88	0.84	0.83	0.91	0.91	0.91	0.84	0.92	0.94	0.93	0.89
RMS vs. rest	0.86	0.87	0.88	0.79	0.90	0.88	0.88	0.86	0.93	0.95	0.92	0.88
NEC vs. rest	0.84	0.85	0.84	0.81	0.90	0.90	0.88	0.84	0.89	0.93	0.92	0.89
ALL vs. rest	0.92	0.93	0.92	0.89	0.94	0.93	0.93	0.89	0.96	0.97	0.96	0.95
NEPB vs. rest	0.91	0.90	0.91	0.89	0.98	0.97	0.96	0.96	0.98	0.98	0.96	0.97
NEUB vs. rest	0.94	0.94	0.93	0.92	0.97	0.95	0.95	0.94	0.98	0.98	0.97	0.97

Table 2: Results of the one vs. one classification for each individual classifier

	One vs. One											
	peptide				<i>N</i> -glycan				peptide and <i>N</i> -glycan combined			
	GB	SVM	KNN	LDA	GB	SVM	KNN	LDA	GB	SVM	KNN	LDA
EWS vs. RMS	0.84	0.82	0.82	0.77	0.86	0.86	0.84	0.82	0.94	0.95	0.9	0.94
EWS vs. NEC	0.83	0.82	0.85	0.78	0.92	0.93	0.93	0.91	0.93	0.94	0.93	0.94
EWS vs. ALL	0.89	0.84	0.89	0.83	0.96	0.95	0.93	0.94	0.97	0.97	0.95	0.97
EWS vs. NEPB	0.92	0.89	0.92	0.85	0.99	0.99	0.98	0.98	0.99	0.99	0.97	0.99
EWS vs. NEUB	0.86	0.86	0.86	0.76	0.96	0.95	0.96	0.96	0.97	0.98	0.94	0.98
RMS vs. NEC	0.88	0.87	0.88	0.81	0.94	0.94	0.89	0.94	0.95	0.96	0.93	0.96
RMS vs. ALL	0.95	0.93	0.93	0.89	0.98	0.98	0.95	0.96	0.97	0.98	0.95	0.98
RMS vs. NEPB	0.87	0.87	0.87	0.85	0.97	0.95	0.94	0.95	0.97	0.98	0.94	0.98
RMS vs. NEUB	0.9	0.89	0.92	0.79	0.98	0.97	0.95	0.98	0.98	0.97	0.95	0.97
NEC vs. ALL	0.85	0.87	0.88	0.84	0.93	0.92	0.9	0.86	0.94	0.94	0.92	0.95
NEC vs. NEPB	0.88	0.88	0.87	0.83	0.99	0.99	0.98	0.99	0.98	0.99	0.97	0.99
NEC vs. NEUB	0.9	0.89	0.92	0.86	0.98	0.97	0.92	0.96	0.98	0.98	0.94	0.98
ALL vs. NEPB	0.93	0.93	0.92	0.89	0.99	1	0.99	0.99	0.99	1	0.98	1
ALL vs. NEUB	0.95	0.93	0.95	0.89	0.99	0.99	0.98	0.97	1	0.99	0.98	0.99
NEPB vs. NEUB	0.86	0.86	0.88	0.88	0.99	0.98	0.97	0.99	0.99	0.99	0.97	0.99

Conclusion & Outlook

- MALDI-MSI of peptide and *N*-glycan profiles has potential to assist in the stratification of small blue round cell tumors and therefore assist in their classification
- Classification using the combined *N*-glycan and peptide data demonstrates greater ability to differentiate between SBRCT classes than by *N*-glycans or peptides individually

- We are currently in the process of identifying differentially expressed peptides (MS/MS)
- Future efforts aim to significantly increase the number of cases and to include more entities

References

- Dubei, D., Bertozzi, C. Glycans in cancer and inflammation — potential for therapeutics and diagnostics. Nat. Rev. Drug Discov. 4, (2005)
- Drake, R.R., et al. In Situ Imaging of *N*-Glycans by MALDI Imaging Mass Spectrometry of Fresh or Formalin-Fixed Paraffin-Embedded Tissue. Curr. Protoc. Protein Sci., (2018)
- Ly, A., et al. Site-to-Site Reproducibility and Spatial Resolution in MALDI-MSI of Peptides from Formalin-Fixed Paraffin-Embedded Samples. Proteomics Clin. Appl. (2019)